J Opt (February 2024) 53(1):206–215
https://doi.org/10.1007/s12596-023-01118-9

Check for updates

RESEARCH ARTICLE

A large effective mode area photonic crystal fiber supporting 134 OAM modes

Yudan Sun[1,2] · Wenshu Lu[2] · Qiang Liu[2] · Jingwei Lv[2] · Shengnan Tai[2] · Mingzhu Han[2] · Paul K. Chu[3] · Chao Liu[2]

Received: 7 November 2022 / Accepted: 28 January 2023 / Published online: 1 March 2023

Abstract A novel photonic crystal fiber (PCF) based on silica is designed for stable transmission of orbital angular momentum (OAM) modes. Numerical analysis shows that the PCF can support more than 134 OAM modes in a broad wavelength range of 1200–2000 nm. In addition, it boasts a large effective mode area between 259.97–423.99 μm^2, confinement loss of all the eigenmodes at 10^{-9}–10^{-10} dB/m, nonlinear coefficients within 0.47 W^{-1}/km with the minimum being 0.25 W^{-1}/km at 1550 nm. The excellent properties reveal that the PCF has large potential in ultra-high capacity OAM mode division multiplexing for fiber communication systems.

Keywords Photonic crystal fibers · Orbital angular momentum · Large effective mode area · Nonlinear coefficients

✉ Yudan Sun
sunyudan1983@163.com

✉ Chao Liu
msm-liu@126.com

1 College of Mechanical and Electrical Engineering, Daqing Normal University, Daqing 163712, People's Republic of China

2 School of Physics and Electronic Engineering, Northeast Petroleum University, Daqing 163318, People's Republic of China

3 Department of Physics, Department of Materials Science and Engineering, and Department of Biomedical Engineering, City University of Hong Kong, Tat Chee Avenue, Kowloon, Hong Kong, People's Republic of China

Introduction

On the heels of the rapid development of mobile internet technology, the capacity crunch of optical fiber communication systems has become increasingly serious. The multiplexing technology is widely used to tackle the challenge, and in particular, space division multiplexing (SDM) is a promising solution to keep up with the growing capacity demand. SDM uses multiplicity of space channels such as multi-cores or multi-mode fibers [1–4] and orbital angular momentum (OAM) mode division multiplexing (MDM) is an important method to achieve SDM. OAM beams with different topological charge numbers add extra degree of freedom and can be used as the information carriers [5]. The technology has been proven to be suitable for free-space data transmission [6–8]. Theoretically, OAM modes have infinite topological charges and the different OAM modes are orthogonal to each other so that the method can improve the capacity and efficiency in optical communication [9].

In order to achieve stable transmission of OAM modes, researchers have designed different kinds of optical fibers operating at near-infrared or terahertz band such as hexagonal lattice PCFs [10], microstructure ring fibers [11, 12], and doped fibers [13, 14]. The ring core photonic crystal fiber can transmit OAM modes better and with improved propagation characteristics if the structure is optimized. So far, many PCFs have been proposed to support transmission of OAM modes [15, 16]. For example, Zhang et al. have proposed the OAM fiber family based on the circular photonic crystal fiber (C-PCF) structure to support up to 42 OAM modes. Zhang et al. have demonstrated a circular photonic crystal fiber for 110 OAM modes [3], but this type of PCF requires a larger refractive index difference between the core and cladding. The conventional methods use high refractive index-doped ring cores [17, 18] or background materials [19]. For example, Kuiri designed a PCF with a high index ring of lithium niobate (LiNbO3) in the background layer of silica, it can support 124 orbital angular momentum modes at 1.55 μm [20]. Another way is to design cladding air holes to increase the air-filling fraction [21], but the PCFs frequently process a narrower ring core and smaller mode area. Although large effective mode area fibers have advantages such as the low nonlinearity, low loss, and bending resistance [12, 22, 23], those supporting OAM modes have rarely been reported and most of the effective mode area is less than 100 μm^2. For example, the reported maximum effective mode areas are 50.54 μm^2 ($HE_{8,1}$) and 70.19 μm^2 ($HE_{13,1}$) at 1.55 μm [24, 25] and the effective mode areas are only 60 ~ 85 μm^2 [26], 78.03 μm^2–88.65 μm^2 [27], and 70–90 μm^2 [28].

In this paper, we describe a large effective mode area photonic crystal fiber that support transmission of 134 OAM modes in the broad wavelength range of 1200–2000 nm. The PCF composed of pure silica consists of four layers of pores in the cladding. The effective mode areas of all the eigenmodes are above 270 μm^2, and the maximum is 391.90 μm^2 at a wavelength of 1.55 μm. The nonlinear coefficients are within 0.47 W^{-1}/km, and the confinement losses are 10^{-9}–10^{-11} dB/m with relatively flat dispersion variations.

Structure

The cross-sectional schematic of the PCF is depicted in Fig. 1. It comprises 4 rings of air holes in the cladding and a large air hole in the center. From inside to outside, the total numbers of the air holes are $N_1 = 72$, $N_2 = 36$, $N_3 = 18$, and $N_4 = 18$ and the corresponding diameters are $d_1 = 2.4$ μm, $d_2 = 6$ μm, $d_3 = 3.2$ μm, and $d_4 = 16$ μm. The distances between the pore center and the fiber center are $l_1 = 32$ μm, $l_2 = 36.2$ μm, $l_3 = 41$ μm, and $l_4 = 47.4$ μm, and the radius of the central air hole is $r = 28$ μm. Pure silica with a refractive index (RI) of 1.444 at 1.55 μm is the fiber materials [5]. The proposed PCF is relatively complex, and it is difficult to produce using traditional stacking method and extrusion method. In recent years, the newly emerged 3D printing technology is used to manufacture optical fiber preform and successfully fabricated hollow PCF [29, 30]. It is believed that the proposed PCF can also be manufactured in future with the progress of the 3D printing preform technology. The analysis is performed by the full vectorial finite element method (FEM).

The OAM modes supported by the PCF are described by the combination of the vector eigenmodes, and the number of OAM modes is calculated by the following formulas [31]:

$$\begin{cases} OAM^{\pm}_{\pm l,m} = HE^{even}_{l+1,m} \pm jHE^{odd}_{l+1,m} \\ OAM^{\mp}_{\pm l,m} = EH^{even}_{l-1,m} \pm jEH^{odd}_{l-1,m} \end{cases} l > 1 \quad (1)$$

$$\begin{cases} OAM^{\pm}_{\pm l,m} = HE^{even}_{l+1,m} \pm jHE^{odd}_{l+1,m} \\ OAM^{\mp}_{\pm l,m} = TM_{0,m} \pm jTE_{0,m} \end{cases} l = 1, \quad (2)$$

where l is the topological charge indicating the order of the OAM modes, m represents the index in the spiral direction

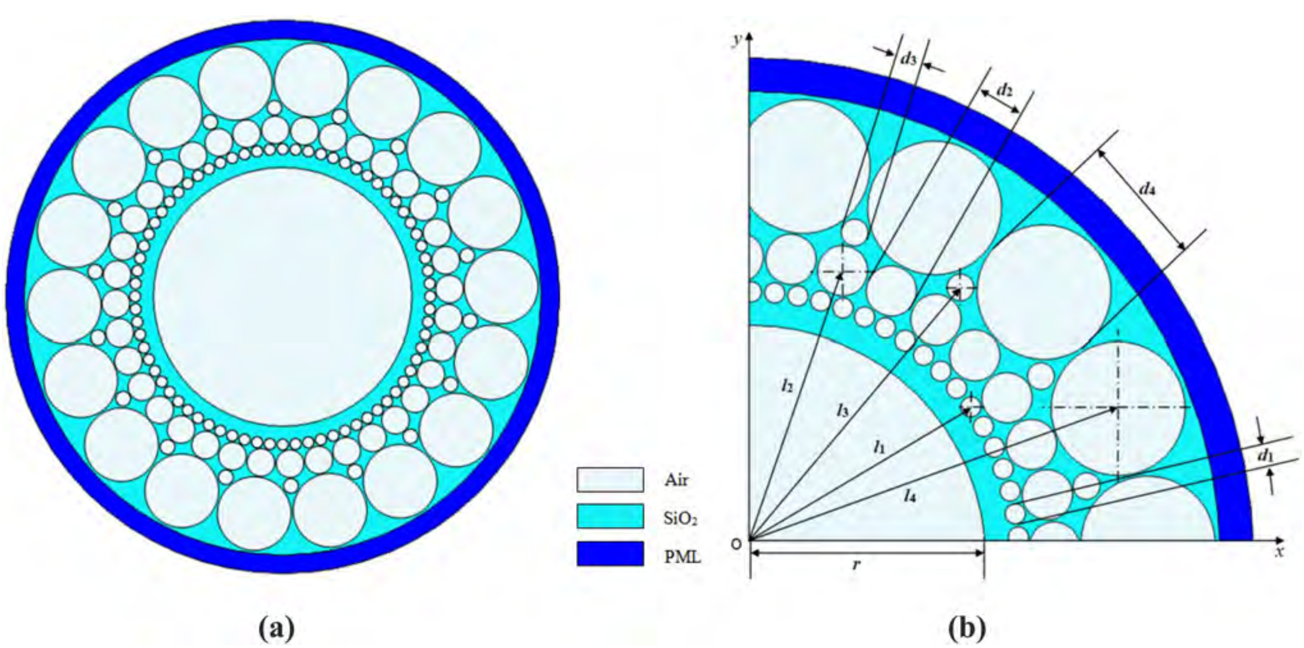

Fig. 1 **a** Cross section of the PCF and **b** parameters of the PCF

and is determined to be 1 in order to avoid accidental degeneracies [32], the superscript "±" is the circular polarization direction of the OAM modes, and the subscript "±" is the rotation direction of the wavefront phase profile. The OAM modes are regarded as the superposition of the even and odd modes of HE or EH with a π/2 phase shift, and the supported OAM modes are listed in Table 1. The total number is 134. Figure 2 shows the electric field intensity distribution of some vector eigenmodes ($HE_{3,1}$, $HE_{14,1}$, $HE_{22,1}$, $HE_{35,1}$, $EH_{1,1}$, $EH_{12,1}$, $EH_{20,1}$ and $EH_{33,1}$) in *z*-direction at 1,550 nm. It is noticed that the electric field intensity of the $HE_{l,1}$ mode is distributed outside of the ring core, and the electric field intensity of the $EH_{l,1}$ mode is distributed inside of the ring core [17]. In order to better analyze the characteristics of

Table 1 OAM modes supported by the PCF

OAM mode	$OAM^{\pm}_{\pm 1,1}$	$OAM^{\pm}_{\pm 2,1}$	$OAM^{\pm}_{\pm 3,1}$	$OAM^{\pm}_{\pm 4,1}$	$OAM^{\pm}_{\pm 5,1}$	$OAM^{\pm}_{\pm 6,1}$	$OAM^{\pm}_{\pm 7,1}$
HE mode	$HE_{2,1}$	$HE_{3,1}$	$HE_{4,1}$	$HE_{5,1}$	$HE_{6,1}$	$HE_{7,1}$	$HE_{8,1}$
EH mode	–	$EH_{1,1}$	$EH_{2,1}$	$EH_{3,1}$	$EH_{4,1}$	$EH_{5,1}$	$EH_{6,1}$
OAM mode	$OAM^{\pm}_{\pm 8,1}$	$OAM^{\pm}_{\pm 9,1}$	$OAM^{\pm}_{\pm 10,1}$	$OAM^{\pm}_{\pm 11,1}$	$OAM^{\pm}_{\pm 12,1}$	$OAM^{\pm}_{\pm 13,1}$	$OAM^{\pm}_{\pm 14,1}$
HE mode	$HE_{9,1}$	$HE_{10,1}$	$HE_{11,1}$	$HE_{12,1}$	$HE_{13,1}$	$HE_{14,1}$	$HE_{15,1}$
EH mode	$EH_{7,1}$	$EH_{8,1}$	$EH_{9,1}$	$EH_{10,1}$	$EH_{11,1}$	$EH_{12,1}$	$EH_{13,1}$
OAM mode	$OAM^{\pm}_{\pm 15,1}$	$OAM^{\pm}_{\pm 16,1}$	$OAM^{\pm}_{\pm 17,1}$	$OAM^{\pm}_{\pm 18,1}$	$OAM^{\pm}_{\pm 19,1}$	$OAM^{\pm}_{\pm 20,1}$	$OAM^{\pm}_{\pm 21,1}$
HE mode	$HE_{16,1}$	$HE_{17,1}$	$HE_{18,1}$	$HE_{19,1}$	$HE_{20,1}$	$HE_{21,1}$	$HE_{22,1}$
EH mode	$EH_{14,1}$	$EH_{15,1}$	$EH_{16,1}$	$EH_{17,1}$	$EH_{18,1}$	$EH_{19,1}$	$EH_{20,1}$
OAM mode	$OAM^{\pm}_{\pm 22,1}$	$OAM^{\pm}_{\pm 23,1}$	$OAM^{\pm}_{\pm 24,1}$	$OAM^{\pm}_{\pm 25,1}$	$OAM^{\pm}_{\pm 26,1}$	$OAM^{\pm}_{\pm 27,1}$	$OAM^{\pm}_{\pm 28,1}$
HE mode	$HE_{23,1}$	$HE_{24,1}$	$HE_{25,1}$	$HE_{26,1}$	$HE_{27,1}$	$HE_{28,1}$	$HE_{29,1}$
EH mode	$EH_{21,1}$	$EH_{22,1}$	$EH_{23,1}$	$EH_{24,1}$	$EH_{25,1}$	$EH_{26,1}$	$EH_{27,1}$
OAM mode	$OAM^{\pm}_{\pm 29,1}$	$OAM^{\pm}_{\pm 30,1}$	$OAM^{\pm}_{\pm 31,1}$	$OAM^{\pm}_{\pm 32,1}$	$OAM^{\pm}_{\pm 33,1}$	$OAM^{\pm}_{\pm 34,1}$	
HE mode	$HE_{30,1}$	$HE_{31,1}$	$HE_{32,1}$	$HE_{33,1}$	$HE_{34,1}$	$HE_{35,1}$	
EH mode	$EH_{28,1}$	$EH_{29,1}$	$EH_{30,1}$	$EH_{31,1}$	$EH_{32,1}$	$EH_{33,1}$	

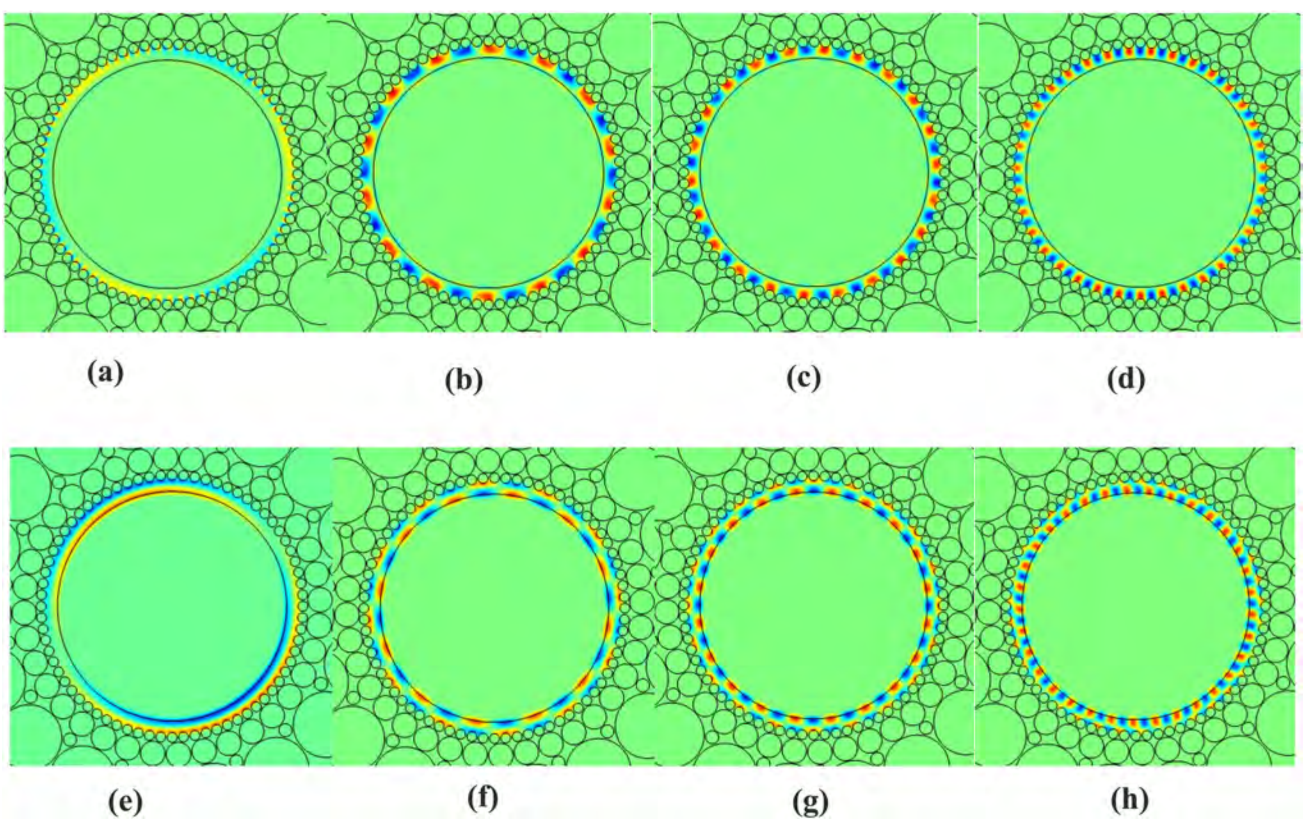

Fig. 2 **a–h** Electric field intensity distributions of the eigenmodes $HE_{3,1}$, $HE_{14,1}$, $HE_{22,1}$, $HE_{35,1}$, $EH_{1,1}$, $EH_{12,1}$, $EH_{20,1}$ and $EH_{33,1}$ in *z*-direction

OAM modes, the phase distribution of the typical $OAM^{+}_{13,1}$ and $OAM^{+}_{34,1}$ modes in the ring core is calculated as shown in Fig. 3. It can be seen that the phase distribution of the ring core shows clear periodic variation and smaller phase distortion. It means that the proposed PCF can keep a high OAM mode quality.

In our efforts to optimize the PCF, it is found that the thickness of the ring core and diameter of the first layer air holes affect the number of OAM modes. Therefore, the thickness of the ring core is optimized first by changing the radius r of the central air hole, as shown in Fig. 4a. The OAM mode number increases with r because the smaller the width of the high refractive index ring core, the larger the effective refractive index difference. Figure 4c shows the effective refractive index difference of $HE_{m+1,1}$ and $EH_{m-1,1}$. The OAM mode number is calculated for different wavelengths, as shown in Fig. 4b. The PCF supports less OAM mode number at short wavelength for $r = 27.2$ µm. It is because that the Δn_{eff} between the mode groups decreases with decreasing wavelength. Some higher-order eigenmodes which can constitute OAM modes at longer wavelength cannot meet the condition of $\Delta n_{eff} > 10^{-4}$ at shorter wavelength. For $r = 28.0$ µm, the PCF can support 134 OAM modes in the range of 1.2–2.0 µm, and hence, $r = 28.0$ µm is chosen as the optimal value considering the benefits of more OAM modes and a larger bandwidth.

Similarly, the influence of the diameter d_1 of the first layer air hole on the OAM mode number is derived as shown in Fig. 5a. The OAM mode number increases with d_1 because a larger air hole accentuates the effective refractive index difference. Figure 5c shows the effective refractive index difference of some vector modes for $d_1 = 2.4$ µm and the effective refractive index difference reaches the maximum. Hence, the PCF supports 134 OAM modes transmission in a wider bandwidth of 1.2–2.0 µm, as shown in Fig. 5b. Meanwhile, an excessively large air hole does not fit in the smaller space, and therefore, $d_1 = 2.4$ µm is determined to be the optimal value. In addition, the parameters of d_2, d_3, d_4 have less influence on the supported OAM mode number, and they determine the confinement loss and mode quality. In order to improve the performance of the PCF by increasing the air-filling ratio of the cladding[17, 33], $d_2 = 6$ µm, $d_3 = 3.2$ µm, and $d_4 = 16$ µm are chosen as the optimal values.

Simulation and analysis

Effective refractive index difference

In order to avoid OAM modes degenerating into the $LP_{l,m}$ mode, the effective refractive index difference (Δn_{eff}) between the hybrid modes in the same propagation constant group ($HE_{m+1,1}$ and $EH_{m-1,1}$) needs to be more than 10^{-4} [34]. The difference of the refractive index can be determined by Eq. (3) [35]:

$$\Delta n_{eff} = \left| n_{eff}\left(HE_{l+1,m}\right) - n_{eff}\left(EH_{l-1,m}\right) \right|, \quad (3)$$

where n_{eff} is the effective refractive index, and Δn_{eff} is the difference of the effective refractive indexes. The effective refractive indexes of all vector modes are calculated as shown in Fig. 6. They decrease with increasing wavelength and that of the lower-order mode is larger than that of the higher-order mode at the same wavelength. The PCF thus supports more than 70 vector modes in the wavelength range between 1.2 and 2.0 µm.

The effective refractive index differences Δn_{eff} between the HE and EH modes are plotted in Fig. 7 which shows that Δn_{eff} increases with increasing wavelength and the effective refractive index difference of the higher-order modes is smaller than that of the lower-order modes. All

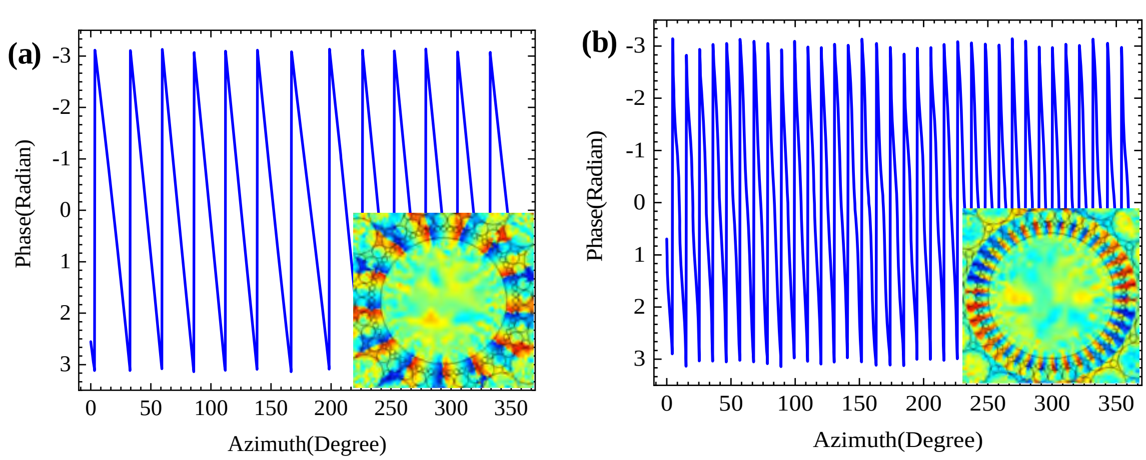

Fig. 3 As $\lambda = 1.55$ µm, the phase distribution of $OAM^{+}_{13,1}$ mode (**a**) and $OAM^{+}_{34,1}$ mode (**b**) in the azimuth direction

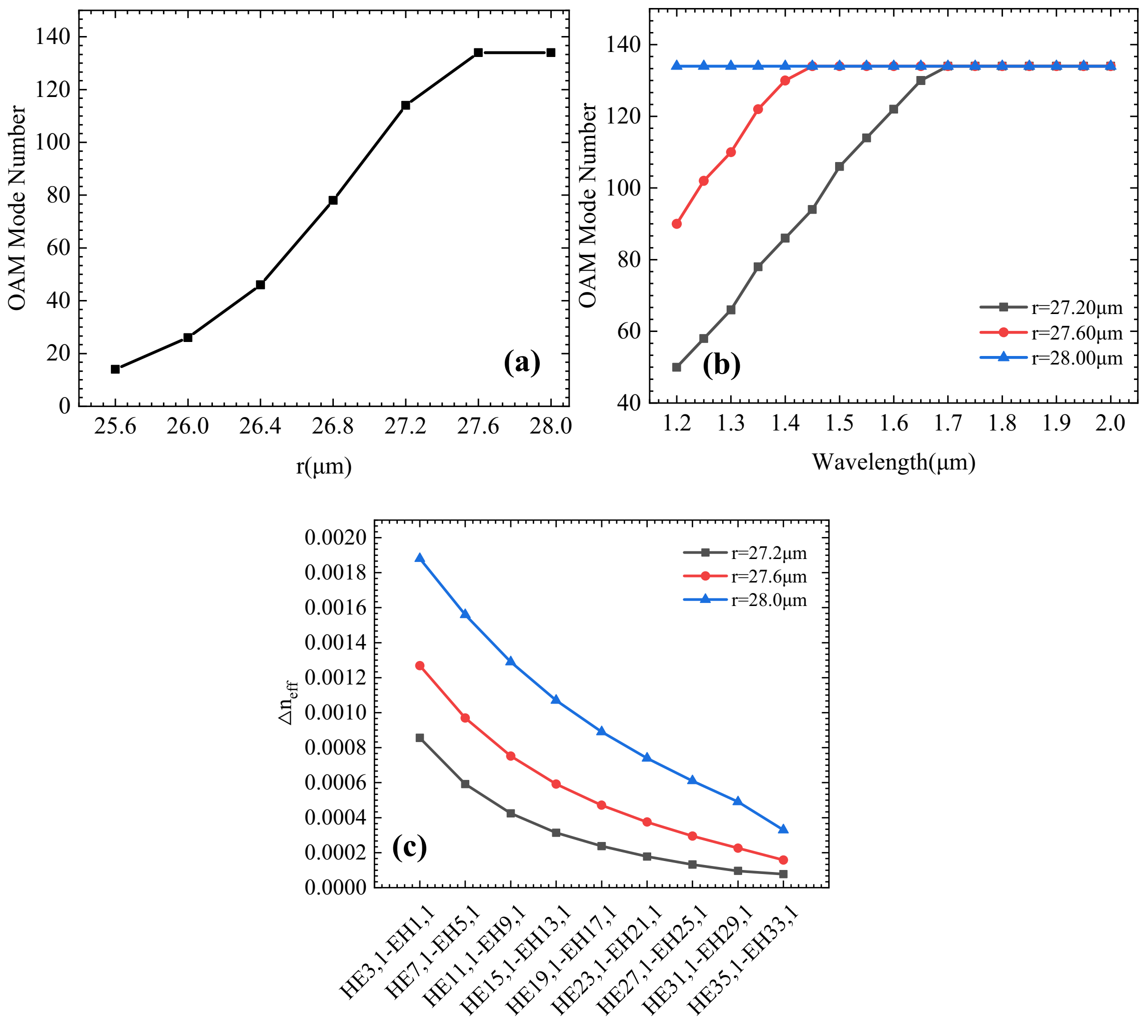

Fig. 4 **a** OAM mode number versus central air hole at $\lambda = 1.55$ μm; **b** OAM mode number at different wavelengths for different *r*; **c** effective refractive index difference of some vector modes for different *r*

the effective refractive index differences are up to 10^{-4} thus avoiding the interactions between the vector modes and ensuring stable transmission of the OAM modes.

Confinement loss

The confinement loss (CL) of the PCF describes the energy attenuation during light transmission in the optical fiber. It produces signal degradation and influences proper transmission of the OAM modes and a smaller CL is beneficial. The CL mainly depends on the arrangement of the air holes and intrinsic materials absorption. If the distribution of air holes in the cladding is denser and the circular symmetry is better, the cladding will have stronger bound on the light field and the corresponding CL will be lower [36]. In order to confine light and reduce CL, the PCF consists of four layers of air holes. The CL is calculated by the following formula:

$$\mathrm{CL} = \frac{20}{\ln 10} k_0 \mathrm{Im}\left(n_{\mathrm{eff}}\right), \tag{4}$$

where $\mathrm{Im}(n_{\mathrm{eff}})$ is the imaginary part of the effective refractive index, and $k_0 = 2\pi/\lambda$ is the wave number in vacuum.

Figure 8 displays the relationship between the confinement loss and wavelength for different eigenmodes. The CL fluctuates greatly with wavelength and most of the CL is concentrated in the range of 10^{-9}–10^{-11} dB/m, which is superior to that of recently reported PCFs with a large effective mode area [35]. This PCF is demonstrated to have low CL boding well for information transmission.

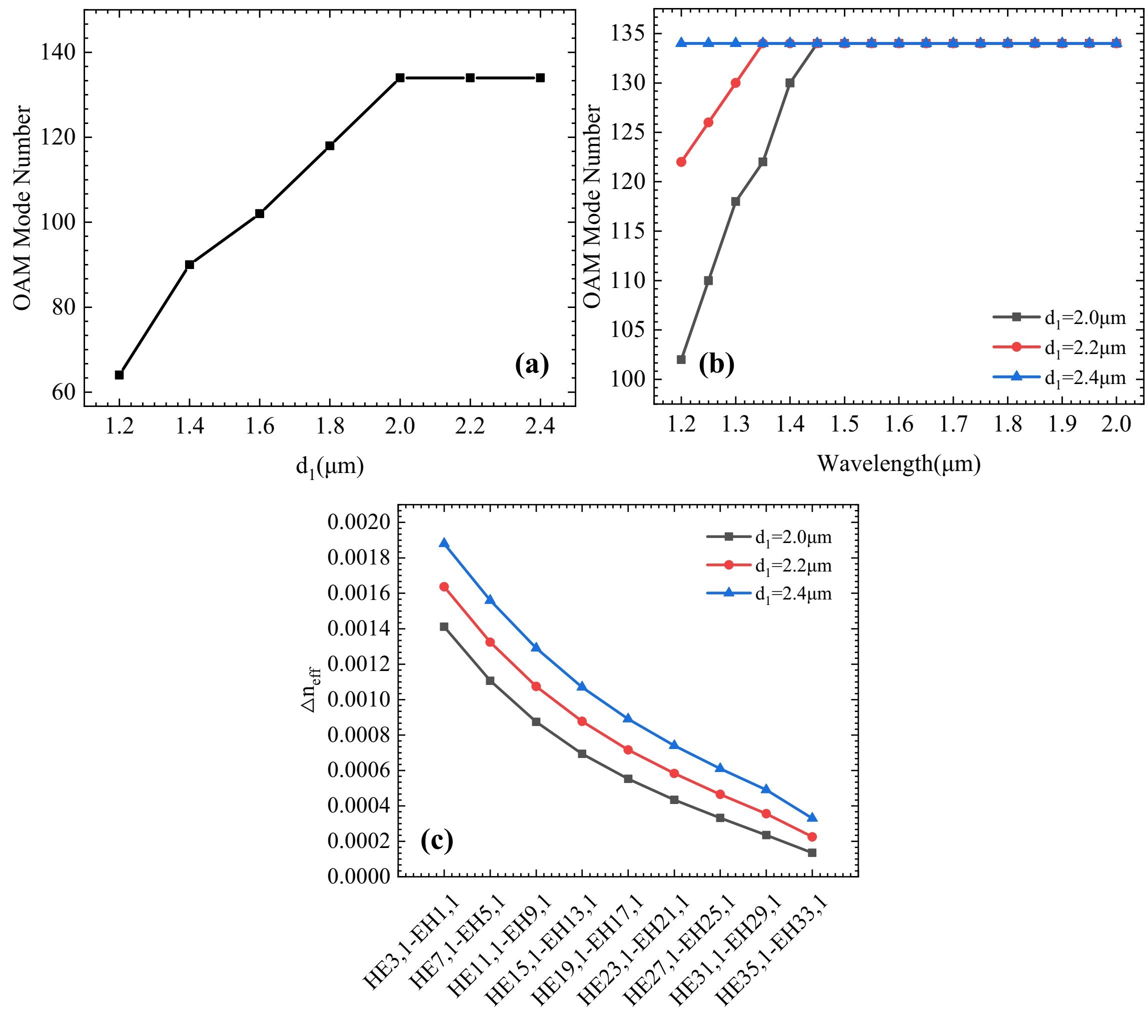

Fig. 5 **a** OAM mode number versus the diameter d_1 of the first layer air hole at $\lambda = 1.55$ μm; **b** OAM mode number at different wavelengths for different d_1; **c** effective refractive index difference of some vector modes for different d_1

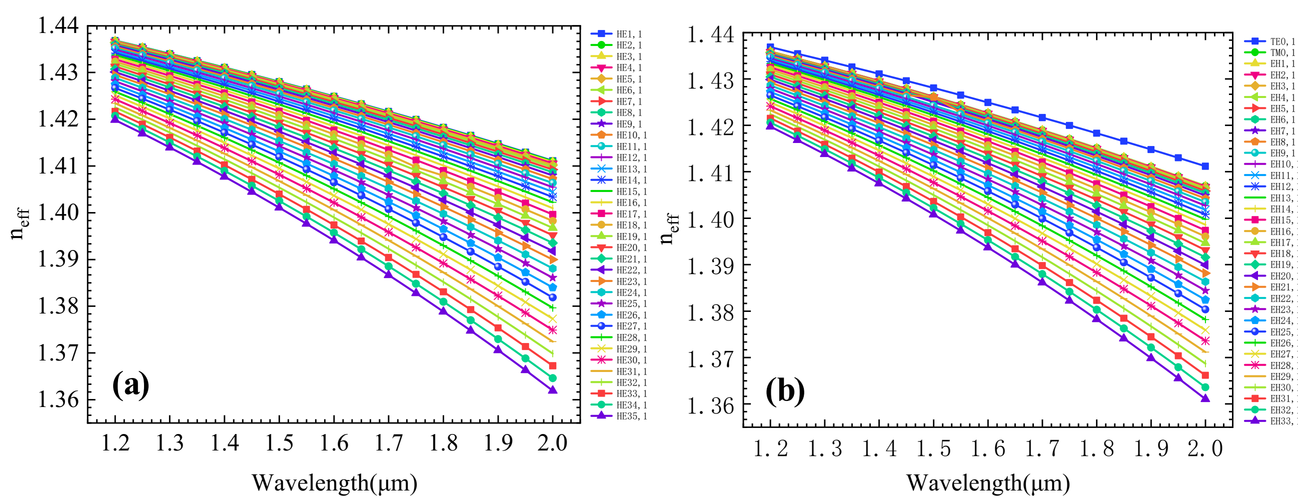

Fig. 6 Effective refractive indexes as a function of wavelength: **a** HE modes and **b** EH modes

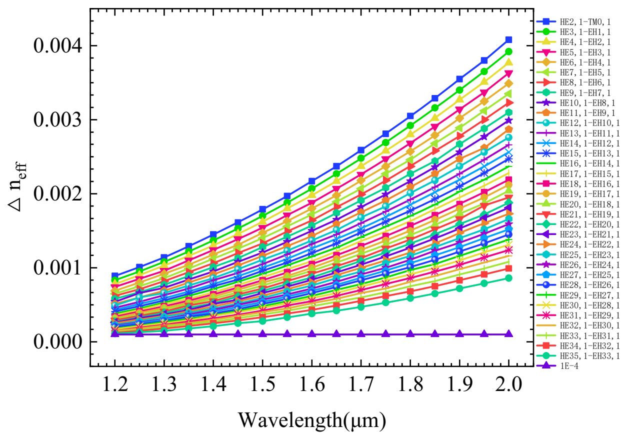

Fig. 7 Effective index separation between the constituent HE and EH modes

Dispersion

Dispersion is one of the inherent characteristics of optical fibers and influences the optical communication capacity. The total dispersion D is determined by materials dispersion D_m and waveguide dispersion D_w as expressed in the following [37]:

$$D(\lambda) = D_w(\lambda) + D_m(\lambda) = -\frac{\lambda}{c}\frac{d^2\mathrm{Re}\left(n_{\mathrm{eff}}\right)}{d\lambda^2} - \frac{\lambda}{c}\frac{d^2 n(\lambda)}{d\lambda^2}, \quad (5)$$

where λ is the wavelength, c is the velocity of light in vacuum, $\mathrm{Re}(n_{\mathrm{eff}})$ is the real part of the effective index of the OAM vector modes, and $n(\lambda)$ is the refractive index of silica and given by Sellmeier equation:

$$n^2(\lambda) = 1 + \frac{A_1\lambda^2}{\lambda^2 - B_1^{\,2}} + \frac{A_2\lambda^2}{\lambda^2 - B_2^{\,2}} + \frac{A_3\lambda^2}{\lambda^2 - B_3^{\,2}}, \quad (6)$$

where $A_1 = 0.696166300$, $A_2 = 0.407942600$, $A_3 = 0.897479400$, $B_1 = 0.0684043$, $B_2 = 0.1162414$, and $B_3 = 9.896161$. Compared with waveguide dispersion, materials dispersion has a smaller impact on the total dispersion, and therefore, materials dispersion is neglected in computing the total dispersion [32].

Figure 9 shows the dispersion of the supported eigenmodes in the wavelength range of 1.2–2.0 μm. The dispersion curves of the supported eigenmodes exhibit monotonous increase with wavelength, and the slope of the dispersion curve of the higher-order eigenmodes is greater than that of lower-order eigenmodes. Furthermore, the dispersion of the EH modes is larger than that of the HE modes for the same order vector modes. At 1.55 μm, the maximum dispersion is 232.33 ps/nm/km ($EH_{33,1}$), lowest dispersion is 79.78 ps/nm/km ($HE_{1,1}$), and the total dispersion variation for all the eigenmodes is less than 210 ps/nm/km.

Effective mode area and nonlinear coefficient

The nonlinear coefficient γ which is another crucial parameter of optical fibers can be calculated by the following equation [38]:

$$\gamma = \frac{2\pi n_2}{\lambda A_{\mathrm{eff}}}, \quad (7)$$

where $n_2 = 2.6 \times 10^{-20}$ m^2/W is the nonlinear refractive index of fused silica, and A_{eff} is the effective mode area defined as follows [39]:

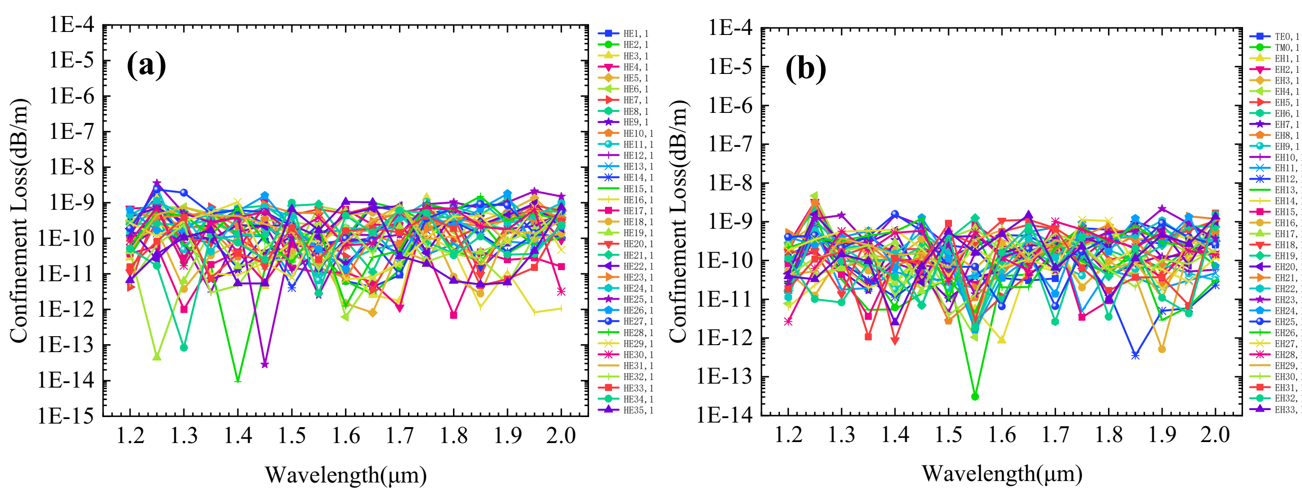

Fig. 8 Confinement loss as a function of wavelength: **a** HE modes and **b** EH modes

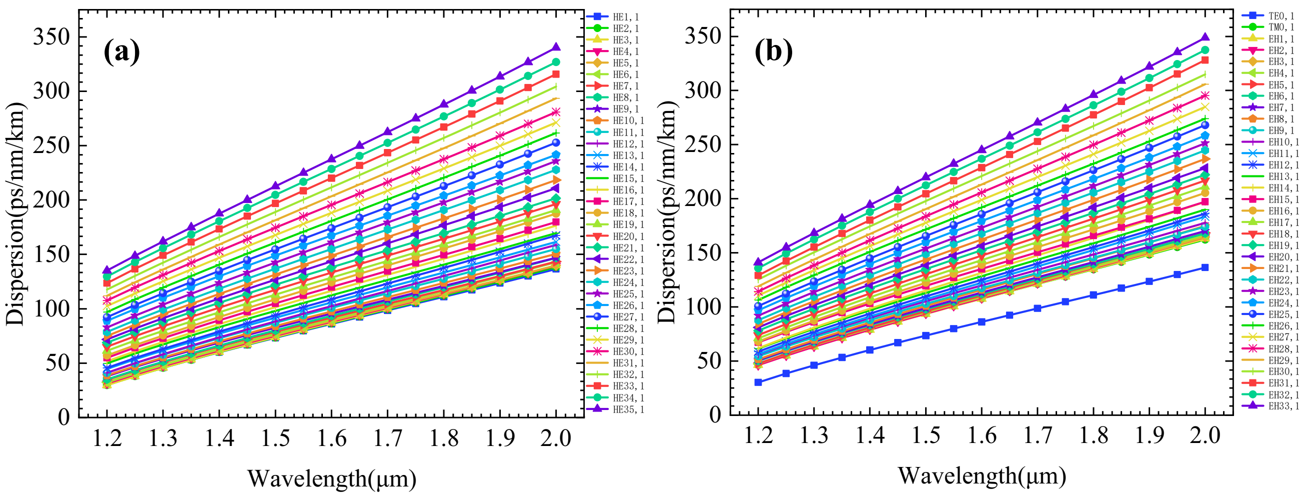

Fig. 9 Dispersion as a function of wavelength: **a** HE modes and **b** EH modes

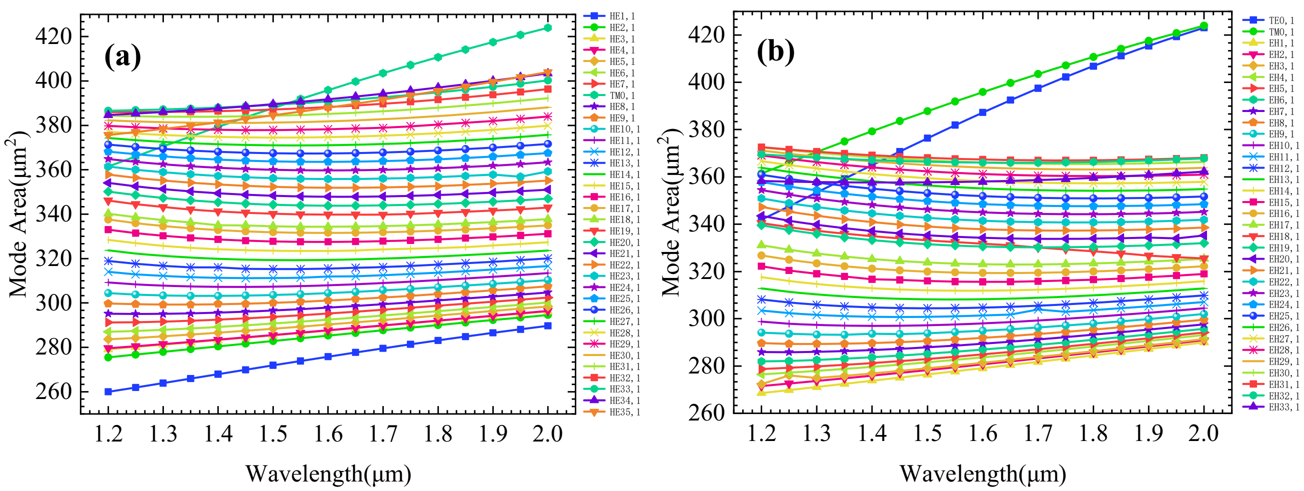

Fig. 10 Effective mode area as a function of wavelength: **a** HE modes and **b** EH modes

$$A_{\mathrm{eff}} = \frac{\left(\iint |\mathrm{E}(x,y)|^2 \mathrm{d}x\mathrm{d}y\right)^2}{\iint |\mathrm{E}(x,y)|^4 \mathrm{d}x\mathrm{d}y}. \quad (8)$$

Figure 10 shows the effective mode area A_{eff} of the supported eigenmodes in the wavelength range of 1.2–2.0 μm. The PCF has a larger effective mode area and all of the effective mode areas are above 259 μm^2 with the maximum being 391.90 μm^2 for $TM_{0,1}$ at 1.55 μm. Owing to the large effective mode area, the PCF may have smaller nonlinear coefficients according to Eq. (7). The calculated nonlinear coefficients are shown in Fig. 11, and the maximum is only 0.47 W^{-1}/km. At 1.55 μm, the nonlinear coefficient is 0.25 W^{-1}/km for the $EH_{30,1}$ mode, which is superior to those reported in Refs. [39] and [40]. The lower nonlinear coefficient mitigates nonlinear optical signal distortion [39] to benefit optical communication. Finally, the performance of the PCF is compared to that of existing PCFs for OAM mode transmission and is shown in Table 2. Our PCF supports more OAM modes in addition to boasting a larger effective mode area and lower nonlinear coefficient.

Conclusion

A large effective mode area PCF which supports 134 OAM modes in the wavelength range of 1.2–2.0 μm is designed and demonstrated. The PCF consists of a ring core with four layers of air holes in the cladding and pure silica as the fiber materials. The characteristics of the PCF are analyzed and optimized by numerical simulation. The PCF

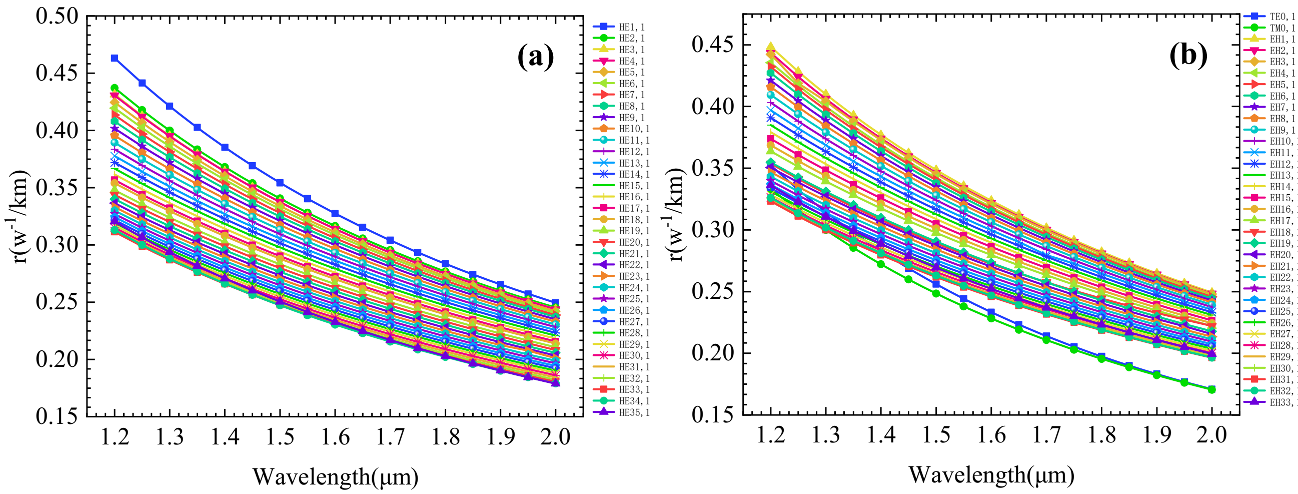

Fig. 11 Nonlinear coefficient as a function of wavelength: **a** HE modes and **b** EH modes

Table 2 Comparison of the performance of our PCF with similar PCFs in the literature

References	Supported OAM modes	Bandwidth (nm)	Confinement loss (dB/m)	nonlinear coefficient (W^{-1}/km)	A_{eff} (μm^2)
[39]	6	400	10^{-6}–10^{3}	12.00–21.00	5.00–8.80
[25]	46	800	10^{-11}–10^{-6}	0.50–2.60	45.00–76.00
[26]	56	1900	10^{-11}–10^{-8}	0.40–4.00	63.00–88.00
[35]	84	600	10^{-12}–10^{-1}	0.80–5.00	32.00–115.00
[40]	30	650	–	1.50–4.25	30.00–55.00
[41]	28	60	–	–	50.00–157.50
Proposed PCF	134	800	10^{-15}–10^{-8}	0.17–0.47	259.97–423.99

shows lower CL (10^{-9}–10^{-10} dB/m), larger effective mode area (259.97–423.99 μm^2), and smaller nonlinear coefficient (0.17–0.47 W^{-1}/km). The results reveal that the PCF has large potential in OAM multiplexing-based optical fiber communication due to the larger communication capacity.

Funding This work was jointly supported by the Provincial Talent Project [ts26180221], Postdoctoral Scientific Research Development Fund of Heilongjiang Province [LBHQ20081], Local Universities Reformation and Development Personnel Training Supporting Project from Central Authorities [140119001], and City University of Hong Kong Strategic Research Grant (SRG) [7005505].

Declarations

Conflict of interest The authors declare no conflicts of interest.

References

1. C. Chen, G.Y. Zhou, G. Zhou, M.N. Xu, Z.Y. Hu, X.M. Xia, J.H. Yuan, A multi-orbital-angular-momentum multi-ring micro-structured fiber with ultra-high-density and low-level cross-talk. Opt. Commun. **368**, 27–33 (2016)
2. H. Zhang, W. Zhang, L. Xi, X. Tang, X. Zhang, X.G. Zhang, A new type circular photonic crystal fiber for orbital angular momentum mode transmission. IEEE Photonic Technol. Lett. **28**, 1426–1429 (2016)
3. L. Zhang, K. Zhang, J. Peng, J. Deng, Y. Yang, J. Ma, Circular photonic crystal fiber supporting 110 OAM modes. Opt. Commun. **429**, 189–193 (2018)
4. A. Kabir, K. Ahmed, M. Hassan, M. Hossain, B.K. Paul, Design a photonic crystal fiber of guiding terahertz orbital angular momentum beams in optical communication. Opt. Commun. **475**, 126192 (2020)
5. W. Wang, C. Sun, N. Wang, H. Jia, A design of nested photonic crystal fiber with low nonlinear and flat dispersion supporting 30+50 OAM modes. Opt. Commun. **471**, 125823 (2020)
6. B. Dutta, N. Sarkar, R. Atta, B. Kuiri, B. Kuiri, S. Santra, A.S. Patra, 640 Gbps FSO data transmission system based on orbital angular momentum beam multiplexing employing optical frequency comb. Opt. Quant. Electron. **54**, 132 (2022)
7. B. Dutta, B. Kuiri, S. Santra, N. Sarkar, I.A. Biswas, R. Atta, A.S. Patra, 100 gbps data transmission based on different l-valued OAM beam multiplexing employing WDM techniques and free space optics. Opt. Quant. Electron. **53**, 515 (2021)
8. B. Dutta, B. Kuiri, N. Sarkar, B. Das, M.D. Sharma, A.S. Patra, Generation of 200 OAM channels for 10 Tbps free space data

transmission using POLMUX based WDM and self-injection locked QD-LD. Opt. Quant. Electron. **54**, 639 (2022)
9. J. Tu, S. Gao, Z. Wang, Z. Liu, C. Yu, H.Y. Tam, C. Lu, Bend-insensitive grapefruit-type holey ring-core fiber for weakly-coupled OAM mode division multiplexing transmission. J. Lightw. Technol. **16**, 4497–4503 (2020)
10. C.Y. Zhao, X.T. Gan, P. Li, L. Fang, L. Han, L.Q. Tu, J.L. Zhao, Design of multicore photonic crystal fibers to generate cylindrical vector beams. J. Lightw. Technol. **34**, 1206–1211 (2016)
11. W. Wang, H. Xu, Q. Yang, F. Zhou, Z. Li, Y. Han, Y. Qi, L. Hou, Large mode area microstructured fiber supporting 56 super-OAM modes. Opt. Express. **27**, 27991–28008 (2019)
12. H.H. Shu, C.M. Qi, C.C. Wei, Z.L. Hong, B.X. Xiao, C. Hu, C.L. Zhi, C.X. Wen, P.L. Ai, Microstructure ring fiber for supporting higher-order orbital angular momentum modes with flattened dispersion in broad waveband. Appl. Phys. B-Lasers O. **125**(11), 197 (2019)
13. B. Kuiri, B. Dutta, N. Sarkar, S. Santra, P. Mandal, K. Mallick, A.S. Patra, Ultra-low loss polymer-based photonic crystal fiber supporting 242 OAM modes with high bending tolerance for multimode THz communication. Results. Phys. **36**, 105464 (2022)
14. B. Kuiri, B. Dutta, N. Sarkar, S. Santra, P. Mandal, K. Mallick, A.S. Patra, Design and optimization of photonic crystal fiber with low confinement loss guiding 98 OAM modes in THz band. Opt. Fiber. Technol. **68**, 102752 (2022)
15. T. Arsène, Y. Jean, D. Michel, B. Géraud, B. Karen, V. Antoine, R.A. Esben, B. Laurent, Ring-core photonic crystal fiber for propagation of OAM modes. Opt. Lett. **44**(7), 1611–1614 (2019)
16. H. Zhang, X.G. Zhang, H. Li, Y.F. Deng, X. Zhang, L.X. Xi, X.F. Tang, W.B. Zhang, A design strategy of the circular photonic crystal fiber supporting good quality orbital angular momentum mode transmission. Opt. Commun. **397**, 59–66 (2017)
17. Q. Ma, A. Luo, W. Hong, Numerical study of photonic crystal fiber supporting 180 orbital angular momentum modes with high mode quality and flat dispersion. J. Lightw. Technol. **39**(9), 2971–2979 (2021)
18. Q. Liu, S. Wen, Y.D. Sun, J.W. Lv, W. Liu, C. Liu, S.N. Tai, B.W. Li, J. Zhao, Y. Jiang, T. Sun, P.K.D. Chu, A novel photonic quasi-crystal fiber for transmission of orbital angular momentum modes. Optik **254**, 168446 (2022)
19. Z.A. Hu, Y.Q. Huang, A.P. Luo, H. Cui, Z.C. Luo, W.C. Xu, Photonic crystal fiber for supporting 26 orbital angular momentum modes. Opt. Express **24**(15), 17285–17291 (2016)
20. B. Kuiri, B. Dutta, N. Sarkar, S. Santra, R. Atta, A.S. Patra, Development of photonic crystal fiber supporting 124 OAM modes with flat dispersion and low confinement loss. Opt. Quant. Electron. **54**, 527 (2022)
21. S. Hong, Y.S. Lee, H. Choi, C. Quan, Y. Li, S. Kim, K. Oh, The PCF design for more number of OAM modes up to 101 by increasing the number of air-holes. Proceedings of SPIE - The International Society for Optical Engineering **11141**, 126–128 (2019)
22. N. Muduli, H.K. Padhy, An optimized configuration of large mode field area PMMA photonic crystal fiber with low bending loss: a new approach. J. Mater. Sci: Mater. El. **27**(2), 1906–1912 (2016)
23. E. Liu, W. Tan, B. Yan, Broadband ultra-flattened dispersion, ultra-low confinement loss and large effective mode area in an octagonal photonic quasi-crystal fiber. J. Opt. Soc. Am. A **35**(3), 431–436 (2018)
24. W. Tian, H. Zhang, X.G. Zhang, L.X. Xi, W.B. Zhang, X.F. Tang, A circular photonic crystal fiber supporting 26 OAM modes. Opt. Fiber Technol. **30**, 184–189 (2016)
25. X. Bai, H. Chena, H. Yang, Design of a circular photonic crystal fiber with square air-holes for orbital angular momentum modes transmission. Optik **158**, 1266–1274 (2018)
26. F. Israk, A. Razzak, K. Ahmed, Ring-based coil structure photonic crystal fiber for transmission of Orbital Angular Momentum with large bandwidth: Outline, investigation and analysis. Opt. Commun. **473**, 126003 (2020)
27. R. Alaaeddine, F. Habib, C. Saleh, M. Mohsen, Design of novel circular lattice photonic crystal fiber suitable for transporting 48 OAM modes. Optoelectron. Lett. **17**(8), 0501–0506 (2021)
28. Q. Liu, S.N. Tai, W. Lu, T. Sun, P.K. Chu, Design of pure silica-based photonic crystal fiber for supporting 114 OAM modes transmission. J. Optics-UK **23**(9), 095701 (2021)
29. Y. Luo, J. Canning, J. Zhang, G. Peng, Toward optical fibre fabrication using 3D printing technology. Opt. Fiber Technol. **58**, 102299 (2020)
30. J. Carcreff, F. Cheviré, E. Galdo, R. Lebullenger, J. Troles, Mid-infrared hollow core fiber drawn from a 3D printed chalcogenide glass preform. Opt. Mater. Express **11**(1), 198–209 (2021)
31. J.X. Yang, H. Zhang, X.G. Zhang, Z. Chen, L.X. Xi, W.B. Zhang, A hollow-core circular photonic crystal fiber mode selective coupler for generating orbital angular momentum modes. Opt. Fiber Technol. **64**(7), 102543 (2021)
32. F.A. Al-Zahrania, M. Hassan, Enhancement of OAM and LP modes based on double guided ring fiber for high capacity optical communication. Alex. Eng. J. **60**(6), 5065–5076 (2021)
33. S. Hong, Y.S. Lee, H. Choi, C. Quan, Y. Li, S. Kim, K. Oh, Hollow silica photonic crystal fiber guiding 101 orbital angular momentum modes without phase distortion in C+L Band. J. Lightw Technol. **38**(5), 1010–1018 (2020)
34. W.C. Wang, N. Wang, K.Y. Li, Z.H. Geng, H.Z. Jia, A novel dual guided modes regions photonic crystal fiber with low crosstalk supporting 56 OAM modes and 4 LP modes. Opt. Fiber Technol. **57**, 102213 (2020)
35. L.J. Zhao, H.Y. Zhao, Z.N. Xu, R.Y. Liang, A design of novel photonic crystal fiber with low and flattened dispersion for supporting 84 orbital angular momentum modes. Commun. Theor. Phys. **73**(8), 085501 (2021)
36. E.X. Liu, S.W. Liang, J.J. Liu, Double-cladding structure dependence of guiding characteristics in six-fold symmetric photonic quasi-crystal fiber. Superlattice Microstruct. **130**, 61–67 (2019)
37. E. Liu, B. Yan, J.L. Xie, Y.C. Peng, F. Gao, J.J. Liu, Dispersion compensation for orbital angular momentum mode based on circular photonic crystal fiber. J. Phys. D Appl. Phys. **54**(43), 435104 (2021)
38. Z. Huo, E. Liu, J. Liu, Hollow-core photonic quasicrystal fiber with high birefringence and ultra-low nonlinearity. Chin. Opt. Lett. **18**(3), 21–26 (2020)
39. E.X. Liu, W. Tan, B. Yan, J.L. Xie, R. Ge, J.J. Liu, Robust transmission of orbital angular momentum mode based on a dual-cladding photonic quasi-crystal fiber. J. Phys. D Appl. Phys. **52**, 325110 (2019)
40. L. Zhang, Y. Meng, Design and analysis of a photonic crystal fiber supporting stable transmission of 30 OAM modes. Opt. Fiber Technol. **61**(15), 102423 (2021)
41. M. Zhu, W.B. Zhang, L.X. Xi, X.F. Tang, X.G. Zhang, A new designed dual-guided ring-core fiber for OAM mode transmission. Opt. Fiber Technol. **25**, 58–63 (2015)

Publisher's Note Springer Nature remains neutral with regard to jurisdictional claims in published maps and institutional affiliations.